Featured in Physics

Magnifying the Wave Function of Interacting Fermionic Atoms

Sandra Brandstetter,[*,†] Carl Heintze,[*] Paul Hill, Philipp M. Preiss,[‡] Maciej Gałka, and Selim Jochim
Physikalisches Institut der Universität Heidelberg, Im Neuenheimer Feld 226, 69120 Heidelberg, Germany

(Received 20 November 2024; accepted 17 June 2025; published 2 September 2025; corrected 9 October 2025)

Understanding many body systems is a key challenge in physics. Single atom resolved imaging techniques have unlocked access to microscopic correlations in ultracold quantum gases. However they cannot be used when the relevant length scales are obscured by the resolution of the detection technique. We present a matter wave magnification scheme, based on evolutions in optical potentials, tailored to magnify the wave function of atoms, such that all length scales can be resolved. To showcase this method, we image atoms in the strongly interacting regime, establishing a new way to characterize correlated systems.

DOI: 10.1103/wdjr-m2hg

Access to high-order correlation functions has become an essential tool in the quest to obtain a deeper understanding of strongly correlated many-body systems. To this end, a vast toolbox for the microscopy of ultracold atoms with single atom and spin resolution has been developed, allowing the in-depth exploration of both lattice systems—using quantum gas microscopes [1]—and continuous systems [2–5]. This toolbox has, for example, been employed in the experimental microscopic observation of the superfluid-Mott insulator transition [6,7], the demonstration of topological quantum states [8,9], and quantum computing with neutral atoms [10].

However, direct imaging is not possible in systems where the interparticle spacing is on the order of the optical resolution. Conceptually, there are two ways to study such systems: either by using superresolution techniques with subwavelength resolution [11,12] or by magnifying the system prior to imaging in a way that preserves the correlations between constituents. This has been achieved using an accordion lattice [13] and by using matter wave optics techniques [14–18].

In this Letter we demonstrate the realization of a matter wave microscope for continuous systems in two dimensions. We magnify the wave function of few ultracold atoms by a factor of about 50, which—in combination with our established free space single atom and spin resolved imaging technique [3,19]—enables access to correlations of arbitrary order. We characterize the performance of the matterwave microscope using the noninteracting harmonic oscillator ground state as a test target and demonstrate its capabilities by imaging a strongly interacting system with single atom and spin resolution in real space.

Matter wave magnification is achieved by two subsequent rotations of the wave function in phase space [17], which are realized by a time evolution in two harmonic potentials, each described by $U_{1,2} = 1/2m\omega_{1,2}^2 x^2$. Here, m is the mass of the particles, $\omega_{1,2}$ is the angular frequency of the respective harmonic oscillator and x is the position in the two-dimensional plane to be imaged. In the Heisenberg picture, the time evolution of the single particle, real and momentum space operators—$\hat{x}$ and $\hat{p}$, respectively—in a harmonic potential are given by

$$\begin{bmatrix} \hat{x}(t) \\ \hat{p}(t) \end{bmatrix} = \begin{bmatrix} \cos\,\omega t & \frac{1}{m\omega}\sin\,\omega t \\ -m\omega\,\sin\,\omega t & \cos\,\omega t \end{bmatrix} \begin{bmatrix} \hat{x}(0) \\ \hat{p}(0) \end{bmatrix}. \quad (1)$$

These equations also apply to the many body case if the system is noninteracting. At $t = (T/4) = \frac{1}{4}(2\pi/\omega)$ the rotation is equivalent to a Fourier transform scaled by $m\omega$, which maps $\hat{x}$ to $\hat{p}$, and vice versa. Therefore, two subsequent rotations in traps with frequencies ω_1 and ω_2 lead to a magnification of the matter wave by a factor of $M = (\omega_1/\omega_2)$. The magnification scheme is illustrated in Fig. 1.

A successful implementation of such a magnification scheme requires that aberrations of the matter wave optics system are well controlled. In practice, this is achieved by making sure that the spatial extent of the wave function $\delta_x(t) = \sqrt{\langle \hat{x}(t)^2 \rangle}$ never probes the part of the potential where significant deviations from a harmonic shape occur.

A possible implementation is the Gaussian potential created by a laser beam,

$$U_G = \tilde{\alpha} I(x) = \tilde{\alpha} \frac{2P}{\pi W^2} \exp\left(\frac{-2x^2}{W^2}\right), \quad (2)$$

where $\tilde{\alpha} = 1/(2\epsilon_0 c)\Re(\alpha)$ is proportional to the real part of the polarizability α, P is the power of the laser beam, and W

[*] These authors contributed equally to this work.
[†] Contact author: brandstetter@physi.uni-heidelberg.de
[‡] Present address: Max Planck Institute of Quantum Optics, Hans-Kopfermann-Straße 1, 85748 Garching, Germany.

 © 2025 American Physical Society

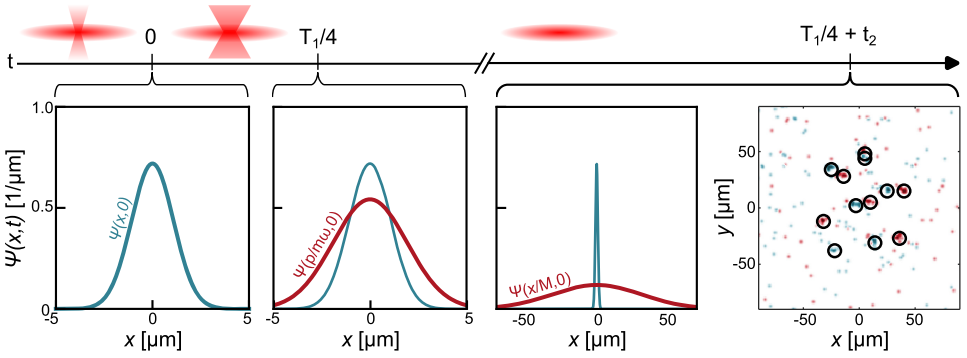


FIG. 1. Matter wave magnification. An initial micro meter sized quantum state—released from an optical tweezer—evolves noninteracting in the magnifier trap, designed to be approximately harmonic at the length scales of interest. After a quarter trap period ($T_1/4$), the wave function has evolved into its Fourier transform, and we obtain $\Psi(x, T_1/4) = \Psi(p/m\omega_1, 0)$. Subsequently, the wave function is transformed back to real space by a time of flight in the weak radial potential of a light sheet trap (2D-OT), resulting in a wave function—$\Psi(x, T_1/4 + t_2) = \Psi(x/M, 0)$—magnified by a factor M allowing the spatially resolved imaging of single atoms as shown on the right. The wave function at each time step is shown in red; the initial wave function is shown in blue for reference. The sequence of optical traps is illustrated by the symbols above the timeline.

is the beam waist in the atom plane. From the series expansion of this potential,

$$U_{\mathrm{G}}(x) = U_{\mathrm{G}}(0)\left(1 - 2\frac{x^2}{W^2} + 2\frac{x^4}{W^4} - \frac{4}{3}\frac{x^6}{W^6} + \mathcal{O}(x^8)\right), \quad (3)$$

it is evident that

$$\delta_{\mathrm{x}}(t) \ll W \quad (4)$$

is required. At $t = 0$ this constraint defines the *field of view* of the matter wave magnifier. During the rotation in phase space, the initial momentum distribution $\delta_{\mathrm{p}}(0)$ is converted into a real space distribution $\delta_{\mathrm{x}}(T_1/4) = \delta_{\mathrm{p}}(0)/m\omega_1$ at $t = T_1/4$. Through Heisenberg's uncertainty the smallest structure sizes in the initial system σ_{x} set a lower limit for the momentum distribution, $\delta_{\mathrm{p}}(0) \geq \hbar/2\sigma_{\mathrm{x}}$. Therefore, the constraint through (4) at $T_1/4$ defines the *diffraction limit* of the matter wave magnifier. The diffraction limit depends on the waist of the Gaussian potential, and on the available laser power [20,25]:

$$\sigma_{\mathrm{x}} \gg \frac{\sqrt{\pi}\hbar W}{4\sqrt{2|\tilde{\alpha}|Pm}}. \quad (5)$$

Note that substantial laser power is required to achieve a diffraction limit much smaller than the field of view.

For the second rotation in phase space, the trap frequency ω_2 is selected such that the magnified smallest structural feature, $M \cdot \sigma_x$, surpasses the optical resolution δ_{psf} of the imaging system. Simultaneously, the magnified wave function must remain within the field of view of the optical imaging setup.

A mapping of the magnified wave function to the initial wave function is possible for times t_2 away from $T_2/4$, when the contribution of the initial momentum is negligible (i.e., when $\cos(\omega_2 t_2)\delta_p(0)/m\omega_1$ is much smaller than the imaging resolution). In this case, the position operator at time $T_1/4 + t_2$ can be approximated as

$$\begin{aligned}\hat{x}(T_1/4 + t_2) &\approx \hat{p}(T_1/4)\frac{1}{m\omega_2}\sin(\omega_2 t_2) \\ &= -\hat{x}(0)\frac{\omega_1}{\omega_2}\sin(\omega_2 t_2). \end{aligned} \quad (6)$$

This results in a magnification factor

$$M = \frac{\omega_1}{\omega_2}\sin(\omega_2 t_2). \quad (7)$$

Our experimental platform is a mesoscopic system of fermionic ^{6}Li atoms in two hyperfine states (denoted as spin up and down) in the ground state of a potential created by two optical traps [20]. A light sheet (2D-OT) confines the atoms along the vertical (z) direction, rendering the system quasi-two-dimensional (2D). A second trap confines the atoms in the radial (r) plane, resulting in a combined potential (OT) with trap frequencies $(\omega_{\mathrm{OT,r}}, \omega_{\mathrm{OT,z}})/2\pi = (1420(2), 7432(3))$ Hz (radial and vertical direction, respectively). Due to the small number of atoms, the characteristic size of our system is set by the harmonic oscillator length, $l_{\mathrm{HO,(r,z)}} = \sqrt{\hbar/m\omega_{\mathrm{OT,(r,z)}}} \approx (1.1, 0.48)$ µm in radial and vertical direction, respectively.

To detect the individual atoms, we utilize a free space, single atom and spin resolved fluorescence imaging technique [3], where each image represents the projection of the wave function on N positions, where N is the number of atoms. The random walk of the atoms during fluorescence, caused by the photon recoil [13], sets the rms width of the point spread function of a single atom to $\delta_{\mathrm{psf}} = 3.96(5)$ µm,

preventing us from resolving the system without further magnification.

We thus magnify the initial system using a matter wave microscope implemented using two Gaussian potentials—tailored for accurate imaging down to the smallest structure sizes of interest. As the magnification sequence begins, the wave function is released from the initial radial confinement; the vertical confinement, provided by the 2D-OT stays on during the entire matter wave magnification. In case of interacting systems, we quench off the interactions at the start of the magnification protocol, simultaneously with the release from the radial confinement. The ability to quench interactions at a timescale much faster than any kinematics is vital for the magnification of interacting systems. Here, the quench is realized through a spin flip to a third, essentially noninteracting hyperfine state [19,20].

The first rotation in phase space is performed by letting the wave function expand in a Gaussian potential for a quarter time period $T_1/4$. The potential is created using a focused laser beam—referred to as magnifier trap (MT)—with trap frequency $\omega_1/2\pi = 1130(10)$ Hz, power $P = 4$ W and waist radius $W \approx 35$ μm—chosen to be much larger than the initial extent of the wave function. Following (4), the field of view is constrained to be much smaller than $W = 20$ μm and condition (5) sets the smallest resolvable structure sizes to $\sigma_x \gg 20$ nm.

Subsequently, we perform the second rotation in phase space by an expansion in a weak radial potential U_2. This potential is a combination of the radial potential of the light sheet $U_{\text{2D-OT}}$ with $\omega_{\text{2D-OT,r}}/2\pi = 16.9(1)$ Hz, and a radial waist of $W_{\text{2D-OT,r}} \approx 600$ μm and the potential created by the magnetic field curvature U_B, with $\omega_{B,r}/2\pi = 10.9(1)$ Hz. The magnetic potential is either repulsive for the low-field seeking state or attractive for the high-field seeking state, such that the total radial frequency $\omega_2/2\pi = 20.2(3), [12.9(3)]$ Hz for high-[low-]field seekers. This configuration of potentials yields a magnification factor of $M = \omega_1/\omega_2 = 56(1)[87(1)]$, depending on the specific conditions. For our typical initial system size (≈4 μm) the magnified wave function remains well within the field of view of the optical imaging setup ($r_{\text{FOV}} = 350$ μm) and the waist of the second trap $W_{\text{2D-OT,r}}$. The smallest structure size of interest in the 2D limit, $l_{\text{HO,z}} = 480$ nm is magnified to $M \cdot l_{\text{HO,z}} \approx 26$ μm[42 μm], far surpassing δ_{psf}.

We characterize the resolution of the matter wave microscope using a single atom in the ground state of the OT as a test target, shown in Fig. 2(a). By varying the radial trap frequency of the OT, we vary the initial system size δr_{prep} and determine the root mean square (rms) width after magnification (δr_{meas}) from many experimental implementations of the same quantum state. Our test target—the harmonic oscillator ground state—exactly matches the Heisenberg uncertainty limit, and is therefore ideal to probe the diffraction limit described above. In an aberration free system, one obtains $\delta r_{\text{meas}} = M \cdot \delta r_{\text{prep}}$ for all δr_{meas}.

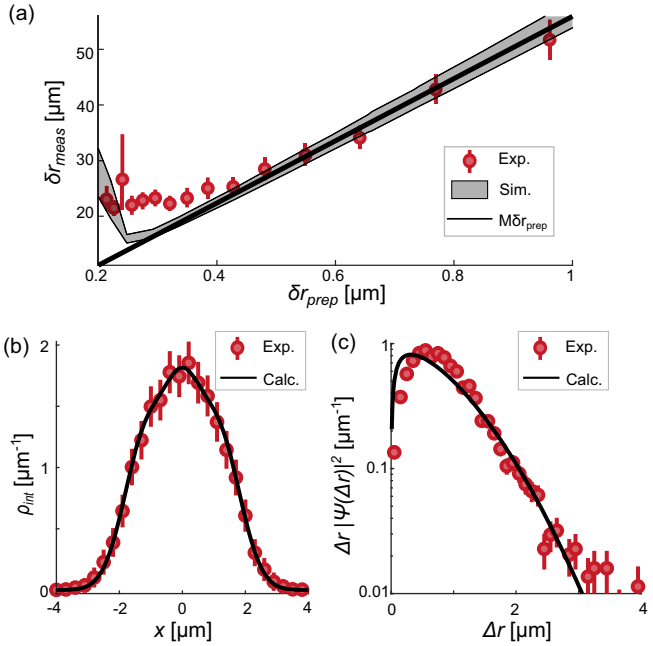


FIG. 2. Performance of the matter wave magnification (a) We vary the initial extent of the wave function δr_{prep} of a single atom in the ground state of the optical tweezer (OT) and determine the position spread δr_{meas} from repeated measurements of the atom position after magnification. The black line shows an aberration free magnification with $M = 56$. The experimental results deviate by a factor of $\sqrt{2}$ from this optimum at $\delta r_{\text{prep}} \approx 300$ nm—setting the resolution. The gray band shows the result of the simulated propagation. (b) Measured (red dots) and calculated (black line) real space density integrated along y direction for 6 non-interacting fermions in the ground state of the OT. (c) Normalized occurrence of measured (red dots) and calculated (black line) distances Δr in a system of 2 particles with a binding energy $E_B/h = 1.5$ kHz in the ground state of a harmonic trap. All error bars show the 95% confidence interval, determined using a bootstrapping technique.

We observe a deviation from this optimum when the condition in (5) is not fulfilled and the matter wave probes the anharmonic regions of the MT. We define the resolution as the point where $\delta r_{\text{meas}} > \sqrt{2} M \delta r_{\text{prep}}$, resulting in $\delta r_{\text{res}} = 300$ nm. Additionally, we perform a numerical simulation of the phase space trajectories in Gaussian traps [20], which matches the experimental measurements, except for very small δr_{prep}.

We verify the ability of our matterwave microscope to image multiple atoms by comparing the measured and the analytically calculated density of a system of six spin up and six spin down (6 + 6) non-interacting atoms prepared in the ground state of the OT with radial trap frequency $\omega_{\text{OT,r}}/2\pi = 1420(2)$ Hz. We magnify the system and obtain the density distribution from averaging over about 1000 experimental realizations of the same quantum state. The measured density integrated over one spatial direction compared to the calculated integrated density is shown in

Fig. 2(b). The measured density is in very good agreement with the calculated density at all positions, demonstrating that this measurement is not limited by the field of view of the matterwave magnifier. The field of view is thus larger than 4 μm.

To demonstrate that our microscope can be used to image interacting systems we prepare two weakly-bound atoms in the ground state of the optical tweezer. We calculate the relative wave function of two interacting particles in a harmonic oscillator potential according to [26], again allowing us to compare our measurements to a known target. Using a Feshbach resonance [27] we set the binding energy [26] to $E_B/h = 1.5$ kHz, with an associated binding length $r_B = \sqrt{\hbar^2/2mE_B} \sim 750$ nm. We obtain a histogram, shown in Fig 2(c), of relative distances of the two particles from many experimental implementations. The experimental measurements and the theoretical expectation are in good agreement, except at very small distances where we are limited by the resolution of the matter wave magnifier.

The matter wave magnifier can be used to explore a strongly interacting many body system. We prepare $6 + 6$ atoms and set the binding length to $r_B = 750$ nm, as in the calibration above. To observe molecules we increase the mean inter-particle spacing to $1/\sqrt{n} = \sqrt{4\pi\hbar^2/2mE_F} \sim$ 4.5 μm, by reducing the radial trap frequency to $\omega_{OT,r}/2\pi = 180$ Hz. This sets the Fermi energy E_F—approximated using the peak density n of the noninteracting system—to $E_F/h = 540$ Hz.

In Fig. 3(a), we show a randomly chosen snapshot of the magnified wave function. Here, each spin up atom appears paired up with a spin down atom. The average density—obtained from many experimental implementations—is depicted by the red background. The cloud is smaller than in the noninteracting regime [shown in Fig. 3(b)], where the system size is comparable to the Thomas Fermi radius $r_F = \sqrt{2E_F/m\omega_{OT,r}^2}$. Note that a different radial trap frequency was used in the noninteracting regime. The position and momenta are thus scaled to the natural units $l_{HO,r}$ and $p_{HO} = \sqrt{\hbar m\omega_{OT,r}}$ of the initial trap. As this alters the harmonic oscillator length $l_{HO,r}$, the effective resolution in terms of $l_{HO,r}$ is smaller in Fig. 3(a) than in Fig. 3(b).

The increase in real space density is accompanied by a decrease in momentum space density as seen in the comparison of Figs. 3(c) (interacting) and 3(d) (noninteracting). The maximum momentum density at a given real space density is governed by Fermi pressure. Beyond that, the momentum density is further decreased by the relative momentum of the pair constituents. A more in-depth analysis of the correlations in momentum space can be found in [19]. The measurements in momentum space were obtained by performing a single rotation in phase space in the weak radial potential ω_2 [19].

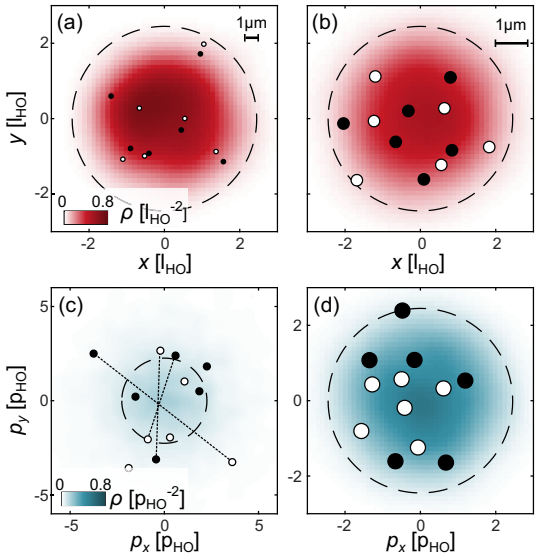


FIG. 3. Fermionic systems in real and momentum space. We image a system of six spin up and six spin down atoms (black/white dots) in real (a),(b) and momentum (c),(d) space, both in the strongly interacting (a),(c) and the noninteracting regime (b),(d). The two dimensional histograms show the density distribution, obtained from averaging over many experimental realizations of the same quantum state. The black and white dots show a single, randomly chosen snapshot of the wave function. The size of the dots represents the resolution. The dashed circles show the Thomas Fermi radius (a),(b) and the Fermi momentum (c),(d) calculated from the noninteracting system. The lines connecting atoms of opposite spin and momentum in (c) serve as a guide to the eye to highlight the opposite momentum correlations.

We have demonstrated matter wave microscopy of a few atom quantum state with single atom and spin resolution. This technique allows for the exploration of correlations of arbitrary order in regimes where the length scales of interest are obfuscated by the resolution of the detection technique. We validate the performance by imaging known systems and show the versatility by imaging $6 + 6$ strongly interacting atoms.

Matter wave microscopy allows the in-depth exploration of fermionic pairing with microscopic observables. The technique can also be used to explore more exotic systems such as recently observed [28], weakly bound NaK tetramers. Beyond that, by altering the time in the magnification trap, the matter wave magnification scheme can be extended to measure in arbitrary bases between real and momentum space. This unlocks the possibility of quantum tomography [29,30] and entanglement characterization [31,32] of many body quantum states.

Acknowledgments—This work has been funded by the DFG (German Research Foundation) Project ID 273811115-SFB 1225 ISOQUANT, the Germany's Excellence Strategy EXC2181/1-390900948 (Heidelberg Excellence Cluster STRUCTURES), and the European

Union's Horizon 2020 research and innovation program under Grant Agreement No. 817482 (PASQuanS). This work has been partially financed by the Baden-Württemberg Stiftung.

[1] C. Gross and W. S. Bakr, Quantum gas microscopy for single atom and spin detection, Nat. Phys. **17**, 1316 (2021).

[2] R. Bücker, A. Perrin, S. Manz, T. Betz, C. Koller, T. Plisson, J. Rottmann, T. Schumm, and J. Schmiedmayer, Single-particle-sensitive imaging of freely propagating ultracold atoms, New J. Phys. **11**, 103039 (2009).

[3] A. Bergschneider, V. M. Klinkhamer, J. H. Becher, R. Klemt, G. Zürn, P. M. Preiss, and S. Jochim, Spin-resolved single-atom imaging of ^{6}Li in free space, Phys. Rev. A **97**, 063613 (2018).

[4] M. Schellekens, R. Hoppeler, A. Perrin, J. V. Gomes, D. Boiron, A. Aspect, and C. I. Westbrook, Hanbury Brown twiss effect for ultracold quantum gases, Science **310**, 648 (2005).

[5] J. Verstraten, K. Dai, M. Dixmerias, B. Peaudecerf, T. De Jongh, and T. Yefsah, *In situ* imaging of a single-atom wave packet in continuous space, Phys. Rev. Lett. **134**, 083403 (2025).

[6] W. S. Bakr, A. Peng, M. E. Tai, R. Ma, J. Simon, J. I. Gillen, S. Foelling, L. Pollet, and M. Greiner, Probing the superfluid–to–Mott insulator transition at the single-atom level, Science **329**, 547 (2010).

[7] J. F. Sherson, C. Weitenberg, M. Endres, M. Cheneau, I. Bloch, and S. Kuhr, Single-atom-resolved fluorescence imaging of an atomic Mott insulator, Nature (London) **467**, 68 (2010).

[8] P. Lunt, P. Hill, J. Reiter, P. M. Preiss, M. Gałka, and S. Jochim, Realization of a Laughlin state of two rapidly rotating fermions, Phys. Rev. Lett. **133**, 253401 (2024).

[9] J. Léonard, S. Kim, J. Kwan, P. Segura, F. Grusdt, C. Repellin, N. Goldman, and M. Greiner, Realization of a fractional quantum Hall state with ultracold atoms, Nature (London) **619**, 495 (2023).

[10] D. Bluvstein, S. J. Evered, A. A. Geim, S. H. Li, H. Zhou, T. Manovitz, S. Ebadi, M. Cain, M. Kalinowski, D. Hangleiter, J. P. Bonilla Ataides, N. Maskara, I. Cong, X. Gao, P. Sales Rodriguez, T. Karolyshyn, G. Semeghini, M. J. Gullans, M. Greiner, V. Vuletić, and M. D. Lukin, Logical quantum processor based on reconfigurable atom arrays, Nature (London) **626**, 58 (2023).

[11] M. McDonald, J. Trisnadi, K.-X. Yao, and C. Chin, Super-resolution microscopy of cold atoms in an optical lattice, Phys. Rev. X **9**, 021001 (2019).

[12] S. Subhankar, Y. Wang, T.-C. Tsui, S. L. Rolston, and J. V. Porto, Nanoscale atomic density microscopy, Phys. Rev. X **9**, 021002 (2019).

[13] L. Su, A. Douglas, M. Szurek, A. H. Hébert, A. Krahn, R. Groth, G. A. Phelps, O. Marković, and M. Greiner, Fast single atom imaging for optical lattice arrays, Nat. Commun. **16**, 1017 (2025).

[14] C. Veit, N. Zuber, O. A. Herrera-Sancho, V. S. V. Anasuri, T. Schmid, F. Meinert, R. Löw, and T. Pfau, Pulsed ion microscope to probe quantum gases, Phys. Rev. X **11**, 011036 (2021).

[15] I. Shvarchuck, C. Buggle, D. Petrov, K. Dieckmann, M. Zielonkowski, M. Kemmann, T. Tiecke, W. Von Klitzing, G. Shlyapnikov, and J. Walraven, Bose-Einstein condensation into nonequilibrium states studied by condensate focusing, Phys. Rev. Lett. **89**, 270404 (2002).

[16] S. Tung, G. Lamporesi, D. Lobser, L. Xia, and E. A. Cornell, Observation of the presuperfluid regime in a two-dimensional Bose gas, Phys. Rev. Lett. **105**, 230408 (2010).

[17] P. Murthy, D. Kedar, T. Lompe, M. Neidig, M. Ries, A. Wenz, G. Zürn, and S. Jochim, Matter-wave Fourier optics with a strongly interacting two-dimensional Fermi gas, Phys. Rev. A **90**, 043611 (2014).

[18] L. Asteria, H. P. Zahn, M. N. Kosch, K. Sengstock, and C. Weitenberg, Quantum gas magnifier for sub-lattice-resolved imaging of 3d quantum systems, Nature (London) **599**, 571 (2021).

[19] M. Holten, L. Bayha, K. Subramanian, S. Brandstetter, C. Heintze, P. Lunt, P. M. Preiss, and S. Jochim, Observation of cooper pairs in a mesoscopic two-dimensional Fermi gas, Nature (London) **606**, 287 (2022).

[20] See Supplemental Material at http://link.aps.org/supplemental/10.1103/wdjr-m2hg for more details on the preparation and interaction switch-off, the numerical simulation of the magnification protocol and an analysis of same and opposite spin correlations. The Supplemental Material also includes Refs. [19,21–24].

[21] E. R. I. Abraham, W. I. McAlexander, J. M. Gerton, R. G. Hulet, R. Côté, and A. Dalgarno, Singlet *s*-wave scattering lengths of ^{6}Li and ^{7}Li, Phys. Rev. A **53**, R3713 (1996).

[22] Z. Hadzibabic and J. Dalibard, Two-dimensional bose fluids: An atomic physics perspective, Riv. Nuovo Cimento Soc. Ital. Fis. **34**, 389 (2011).

[23] J. Levinsen and M. M. Parish, Strongly interacting two-dimensional Fermi gases, in *Annual Review of Cold Atoms and Molecules*, edited by K. Madison, K. Bongs, L. Davis, and C. Foot (World Scientific, Singapore, 2015), Vol. 3, Chap. 1, pp. 1–75.

[24] M. Gajda, J. Mostowski, T. Sowiński, and M. Załuska-Kotur, Single-shot imaging of trapped Fermi gas, Europhys. Lett. **115**, 20012 (2016).

[25] Note that choosing a larger trap frequency $\omega \propto \sqrt{P}W^{-2}$ over a larger waist reduces the laser power required, as long as condition (4) is fulfilled.

[26] Z. Idziaszek and T. Calarco, Analytical solutions for the dynamics of two trapped interacting ultracold atoms, Phys. Rev. A **74**, 022712 (2006).

[27] G. Zürn, T. Lompe, A. N. Wenz, S. Jochim, P. S. Julienne, and J. M. Hutson, Precise characterization of ^{6}Li feshbach resonances using trap-sideband-resolved RF spectroscopy of weakly bound molecules, Phys. Rev. Lett. **110**, 135301 (2013).

[28] X.-Y. Chen, S. Biswas, S. Eppelt, A. Schindewolf, F. Deng, T. Shi, S. Yi, T. A. Hilker, I. Bloch, and X.-Y. Luo, Ultracold field-linked tetratomic molecules, Nature (London) **626**, 283 (2024).

[29] C. Gross, H. Strobel, E. Nicklas, T. Zibold, N. Bar-Gill, G. Kurizki, and M. K. Oberthaler, Atomic homodyne detection of continuous-variable entangled twin-atom states, Nature (London) **480**, 219 (2011).

[30] M. O. Brown, S. R. Muleady, W. J. Dworschack, R. J. Lewis-Swan, A. M. Rey, O. Romero-Isart, and C. A. Regal, Time-of-flight quantum tomography of an atom in an optical tweezer, Nat. Phys. **19**, 569 (2023).

[31] A. Bergschneider, V. M. Klinkhamer, J. H. Becher, R. Klemt, L. Palm, G. Zürn, S. Jochim, and P. M. Preiss, Experimental characterization of two-particle entanglement through position and momentum correlations, Nat. Phys. **15**, 640 (2019).

[32] T. Kitagawa, A. Aspect, M. Greiner, and E. Demler, Phase-sensitive measurements of order parameters for ultracold atoms through two-particle interferometry, Phys. Rev. Lett. **106**, 115302 (2011).

[33] F. Serwane, G. Zurn, T. Lompe, T. B. Ottenstein, A. N. Wenz, and S. Jochim, Deterministic preparation of a tunable few-fermion system, Science **332**, 336 (2011).

[34] L. Bayha, M. Holten, R. Klemt, K. Subramanian, J. Bjerlin, S. M. Reimann, G. M. Bruun, P. M. Preiss, and S. Jochim, Observing the emergence of a quantum phase transition shell by shell, Nature (London) **587**, 583 (2020).

Correction: During the production process byline footnote indicators were erroneously assigned and have been fixed.